Numerical Modeling of Convective Columns above a Large Fire in the Atmosphere

I. F. Muzafarov and S. V. Utyuzhnikov

Moscow Physicotechnical Institute, Moscow, Russia

Received July 7, 1994

Abstract – A numerical model is proposed to study the rise of the combustion products above large fires in a stratified atmosphere. The effect of the area of fire on the height of rising of the contaminant is treated. The structure of the convective columns formed during the fire is studied in detail. The effect of turbulent mixing on the altitude of hovering of the contaminant cloud is demonstrated.

INTRODUCTION

A large fire results in the discharge of a large number of aerosol particles in the form of soot and ash emitted into the atmosphere. The emission of the combustion products into the atmosphere may lead to local and regional climatic aftereffects up to a threat of "nuclear winter" [1]. The numerical modeling of the effects of large fires is discussed in a number of papers published in recent years [2 - 7]. In [3 - 5], it is proposed to model the energy release source of a fire by a volume source whose power increases with time by the linear law to some maximum value. In magnitude, the source power corresponded to the case of complete combustion per unit area. The investigations in [3 - 6] made it possible to determine the characteristic values of the flow velocity, altitude of the rise of the cloud of combustion products, amount of aerosol emitted into the atmosphere, as well as the effect of atmospheric humidity on this amount. Gostintsev *et al.* [7] studied the initial phase of formation of fire due to radiation caused by nuclear explosion.

At the same time, the studies [3 - 7] were conducted using the first-order approximation scheme on a rather crude net of the order of 50 × 50 that prevented one from revealing a more detailed structure of flow caused by the fire. In this study, numerical modeling is based on compact schemes of the third order of approximation in space variables [8] on a 41 × 41 net (the points of net crowding together towards the Earth's surface). The approximation in time corresponded to the second order. The numerical algorithm is described in more detail in [9], where the dynamics of formation of gasdynamic flow during a large fire are investigated along with the flow turbulization effect, and the dependence of the flow parameters and structure on the fire center is studied. In [10], it was experimentally found that the extinction of the fire center at a later stage (after hovering of the cloud of fire products) results in a decrease of the hovering altitude. In our paper, the results of [10] have found numerical support.

Balabanov *et al.* [10] experimentally studied the influence of the fire area on the altitude of spreading of a convective cloud. It has been found that, ass long as the characteristic size of the fire center is less than the double altitude of the tropopause, the cloud spreading altitude is in good agreement with the dependence for a point source and, with a further increase of the fire area, the altitude of spreading even decreases somewhat. This result is confirmed in our study.

STATEMENT OF THE PROBLEM

The gas motion in a stratified atmosphere, caused by a fire will be described on the basis of the Navier–Stokes equations averaged according to Reynolds. The system of equations is written in the cylindrical system of coordinates $\{z, r\}$, where z is the coordinate reckoned from the Earth's surface. Assume that the problem has an axial symmetry.

The system of Navier–Stokes equations is written as

$$\frac{\partial}{\partial t}q + \frac{1}{r}\frac{\partial}{\partial x^i}(re^i_{\text{inv}}) + \frac{1}{r}\frac{\partial}{\partial x^i}(r\frac{\mu}{\text{Re}}\tilde{e}^i_{\text{vis}}) = -gf + q^* + \frac{1}{r}\tilde{s}_{\text{inv}} + \frac{1}{r}\frac{\mu}{\text{Re}}\tilde{s}_{\text{vis}}. \quad (1)$$

Here

$$q = \begin{vmatrix} \rho \\ \rho u \\ \rho v \\ E \end{vmatrix}, \quad e^i_{\text{inv}} = \begin{vmatrix} \rho V^i \\ \rho V^i u + p\delta^{i1} \\ \rho V^i v + P\delta^{i2} \\ (E+p)V^i \end{vmatrix},$$

0018-151X/95/3304-0588$12.50 © 1995 МАИК Наука/Interperiodica Publishing

$$\tilde{e}^i_{\text{vis}} = \begin{vmatrix} 0 \\ \frac{2}{3}\frac{1}{r}\frac{\partial(rV^k)}{\partial x^k}\delta^{i1} - \left(\frac{\partial u}{\partial x^i} + \frac{\partial V^i}{\partial x^1}\right) \\ \frac{2}{3}\frac{1}{r}\frac{\partial(rV^k)}{\partial x^k}\delta^{i2} - \left(\frac{\partial v}{\partial x^i} + \frac{\partial V^i}{\partial x^2}\right) \\ \frac{2}{3}\frac{1}{r}\frac{\partial(rV^k)}{\partial x^k}V^i - \left(\frac{\partial V^k}{\partial x^i} + \frac{\partial V^i}{\partial x^k}\right)V^k - \frac{1}{\text{Pr}}\frac{\partial h}{\partial x^i} \end{vmatrix},$$

$$f = \begin{vmatrix} 0 \\ \rho \\ 0 \\ \rho u \end{vmatrix}, \quad q^* = \begin{vmatrix} 0 \\ 0 \\ 0 \\ Q^* \end{vmatrix},$$

$$\tilde{s}_{\text{inv}} = \begin{vmatrix} 0 \\ 0 \\ p \\ 0 \end{vmatrix}, \quad \tilde{s}_{\text{vis}} = \begin{vmatrix} 0 \\ 0 \\ \frac{2}{3}\frac{\partial V^k}{\partial x^k} - \frac{4}{3}\frac{v}{r} \\ 0 \end{vmatrix},$$

$$i = 1, 2; \; k = 1, 2,$$

where q is the vector of independent variables; e^i_{inv} is the vector of nonviscous flows; $\tilde{e}^i_{\text{vis}}$, e^i_{vis}, and b^i are the vectors of viscous flows; f is the vector of external force due to the field of gravity; q^* is the vector of the volume source of energy release; $\tilde{s}_{\text{inv}}$ and $\tilde{s}_{\text{vis}}$ are the source, "nonconservative" terms due to the fact that the system of coordinates $\{z, r\}$ is non-Cartesian. Here and below, the repeating indices are used for summing up.

The following notation is used in (1): t is the time; $\{x^1, x^2\} = \{z, r\}$; ρ is the density; $\{V^1, V^2\} = \{u, v\}$ are the velocity components in the $\{z, r\}$ direction; $E = \rho\left(\varepsilon + \frac{V_k V^k}{2}\right)$ is the total energy; ε is the internal energy; p is the pressure; $h = \varepsilon + p/\rho$ is the enthalpy; g is the free fall acceleration; μ is the viscosity; Q^* is the power of the amount of heat released from external sources per unit volume.

All quantities in (1) are dimensionless. The relationship between the dimensionless values f and dimension f_{phys} is given by $f_{\text{phys}} = f\bar{f}$, where $\bar{f}$ is the dimensionless factor.

The variables in (1) were made dimensionless to the following quantities: $\bar{x}^i = L_0$, where L_0 is some linear dimension characteristic of the problem; $\bar{V}^i = V_0$, where V_0 is some characteristic velocity; $\bar{t} = L/V_0$, $\bar{\rho} = \rho_0$, where ρ_0 is some characteristic density; $\bar{E} = \rho_0 V_0^2$; $\bar{p} = \rho_0 V_0^2$; $\bar{h} = V_0^2$; $\bar{\mu} = \mu_0$, where μ_0 is some characteristic value of the viscosity; $\bar{g} = Lg_0/V_0^2$, where g_0 is the value of free fall acceleration near the Earth's surface; and $\overline{Q^*} = L/\rho_0 V_0^3$.

Equation (1) incorporates the dimensionless numbers Re and Pr,

$$\text{Re} = \frac{\rho_0 V_0 L}{\mu_0}, \quad \text{Pr} = \frac{\mu C_p}{\lambda_t}.$$

Here, C_p is the heat capacity at constant pressure; and λ_t is the thermal conductivity coefficient. It is assumed that the equation of state is as follows:

$$p = (\gamma - 1)\rho\varepsilon, \quad \varepsilon = C_v T,$$

where γ is the adiabatic index (for air, $\gamma = 1.4$); C_v is the heat capacity at constant volume.

The turbulent transfer coefficients were calculated according to the algebraic model of [11] (it was also used in [5, 6]) which, for the axisymmetric case, is written as

$$\mu = \mu_l + \mu_t, \quad \mu_t = \frac{\rho l^2}{2}\left\{\left(\frac{\partial v}{\partial z} + \frac{\partial u}{\partial r}\right)^2 + 2\left[\left(\frac{\partial v}{\partial r}\right)^2 + \left(\frac{\partial u}{\partial z}\right)^2 + \left(\frac{v}{r}\right)^2\right]\right\}^{1/2},$$

$$l = K\left\{(v^2 + u^2)^{1/2} B^{-1/2} + B^{1/2}\left[\left(\frac{\partial^2 v}{\partial r^2} + \frac{1}{r}\frac{\partial v}{\partial r} - \frac{v}{r^2}\right)^2 + \left(\frac{\partial^2 v}{\partial z^2}\right)^2 + \left(\frac{\partial^2 u}{\partial r^2} + \frac{1}{r}\frac{\partial u}{\partial r}\right)^2 + \left(\frac{\partial^2 u}{\partial z^2}\right)^2\right]^{-1/2}\right\},$$

$$B = \left(\frac{\partial v}{\partial r}\right)^2 + \left(\frac{\partial v}{\partial z}\right)^2 + \left(\frac{v}{r}\right)^2 + \left(\frac{\partial u}{\partial r}\right)^2 + \left(\frac{\partial u}{\partial z}\right)^2,$$

where μ_l and μ_t are the coefficients of laminar and turbulent viscosity, respectively; l is the mixing length; and K is the empirical constant. In numerical calculations, we assumed that $K = 0.125$ and $\text{Pr} = 1$.

The energy source was assumed to be a volume with the radius R and height h (which was taken to be 100 m). The volume source intensity Q^* varied linearly with

time up to the value Q^*_{max}, which was attained after 30 min, as in [5, 6]. The source was cut-off after 60 min.

The boundary conditions were preset as follows. On the Earth's surface, three boundary conditions are specified (nonpercolation, sticking, and internal energy condition),

$$u = v = \frac{\partial}{\partial z}\varepsilon = 0.$$

On the axis of symmetry, the conditions of symmetry are set for the thermodynamic functions and z-component of velocity, as well as the condition of vanishing of the r-component of velocity,

$$\frac{\partial}{\partial r}\{\rho, u, \varepsilon\} = v = 0.$$

On the artificial boundaries emerging when the infinite regions are replaced by the finite ones, the characteristic boundary conditions are specified, based on treating the system of determining equations as a locally one-dimensional system near the boundary (the space direction normal to the boundary is analyzed). Then, for the characteristics incoming from the boundary to the region, the boundary condition is determined for the corresponding Riemann invariant α_i, $\alpha_i|_b = \alpha_i|_{b,\,undist}$, and for the outgoing characteristics the compatibility condition is determined [12]. Here, the subscript b means that the function value is taken on the boundary; $\alpha_i|_{b,\,undist}$ is the value of Riemann invariant, calculated by the parameters of the undisturbed atmosphere at the given boundary point.

NUMERICAL MODELING RESULTS

The effect of the fire area on the flow dynamics and on the altitude of rise of the contaminant was studied. The contaminant was considered as "passive", ignoring its mass and diffusive transfer. In so doing, the radius and altitude of the rise of the cloud of fire products were determined by the maximum values of r and z corresponding to the passive contaminant.

The following values of the radius R of the fire center were considered: 5, 8, 11, 22, and 33 km. The maximum energy release from unit area of the surface was $q_m = 5 \times 10^4$ W/m^2.

The atmosphere corresponded to the international standard. When $R = 5$ km (the total power q_f of energy release is 3.9×10^6 MW), the initial stage of fire development is accompanied by air inflow to the fire center in the wall region. In this case, two vortexes are formed oriented in opposite directions and located one above the other (as previously mentioned in [5, 6]), with the lower vortex being slightly shifted to the right. The propagation of contaminant is characterized by the formation of two "tongues," each of which is formed by its "own" vortex. Shown in Figs. 1a and 1b is the contaminant distribution corresponding to the moments of time of 20 and 60 min. It is clearly seen that the top "tongue" overtakes the bottom one, because the former is permanently replenished owing to the rising air flow in the vicinity of the axis of symmetry. The contaminant cloud rises to the maximum altitude of 12 - 13 km in approximately 30 min. This result conforms to the conclusion of [6], where a similar version of fire is treated. In this case, the upper edge of the cloud oscillates near the equilibrium position with a period of 5 - 7 min corresponding to the natural frequency of oscillation of the atmosphere, determined by the Brent–Vasel formula [13]

$$N^2 = \frac{g}{T_e}\left(\frac{dT_e}{dz} + \gamma_a\right),$$

where T_e is the air temperature in the undisturbed atmosphere; and γ_a is the adiabatic temperature gradient. The temperature at the source boundary assumes characteristic values of 380 - 420 K.

The time dependence of the radius of the contaminant cloud (the coordinates of the point having the maximum value of r) and of the maximum altitude of its rise is given in Fig. 2. The formation of three plateaus in the $r_{max}(t)$ relationship is attributed to the rearrangement of flow associated with the extension of first the bottom "tongue" and then the top one. Although the maximum altitude of rise of the contaminant is equal to 13 km, the cloud of the combustion products spreads mainly at the level of 6 - 7 km.

In the case of $R = 8$ km ($q_f = 10^7$ MW), the following singularities take place. In the initial period of time, the formed bottom vortex is not located under the top one but is shifted to the right with the center in the range of 5 km. Therefore, the propagation of the contaminant in the radial direction is governed by the bottom vortex that entraps the combustion products and discharges them into the atmosphere. The maximum altitude of rise of the contaminant is 12 - 14 km. The edge radius reaches 12 km within 40 min, and this is 6 km more than in the preceding version.

The dynamics of formation of gas-dynamic flow at $R = 11$ km ($q_f = 1.9 \times 10^7$ MW) differ significantly from the preceding two. In the initial period of time, three vortexes are formed in the flow, distributed relative to each other in the horizontal direction and having centers approximately corresponding to the values of $r = 1$, 4, 9 km. The velocity field for the moments of time 60 and 90 min is shown in Figs. 3a and 3b.

As seen from the drawings, the flow structure by the moment of time of 90 min is very complex and is characterized by the formation of many vortexes. Such a flow structure is formed mainly after the cloud of combustion products reaches the hovering height. At this stage, the generation of vortexes is governed by the internal gravitational waves. The vortex formation frequency corresponds to the frequency N.

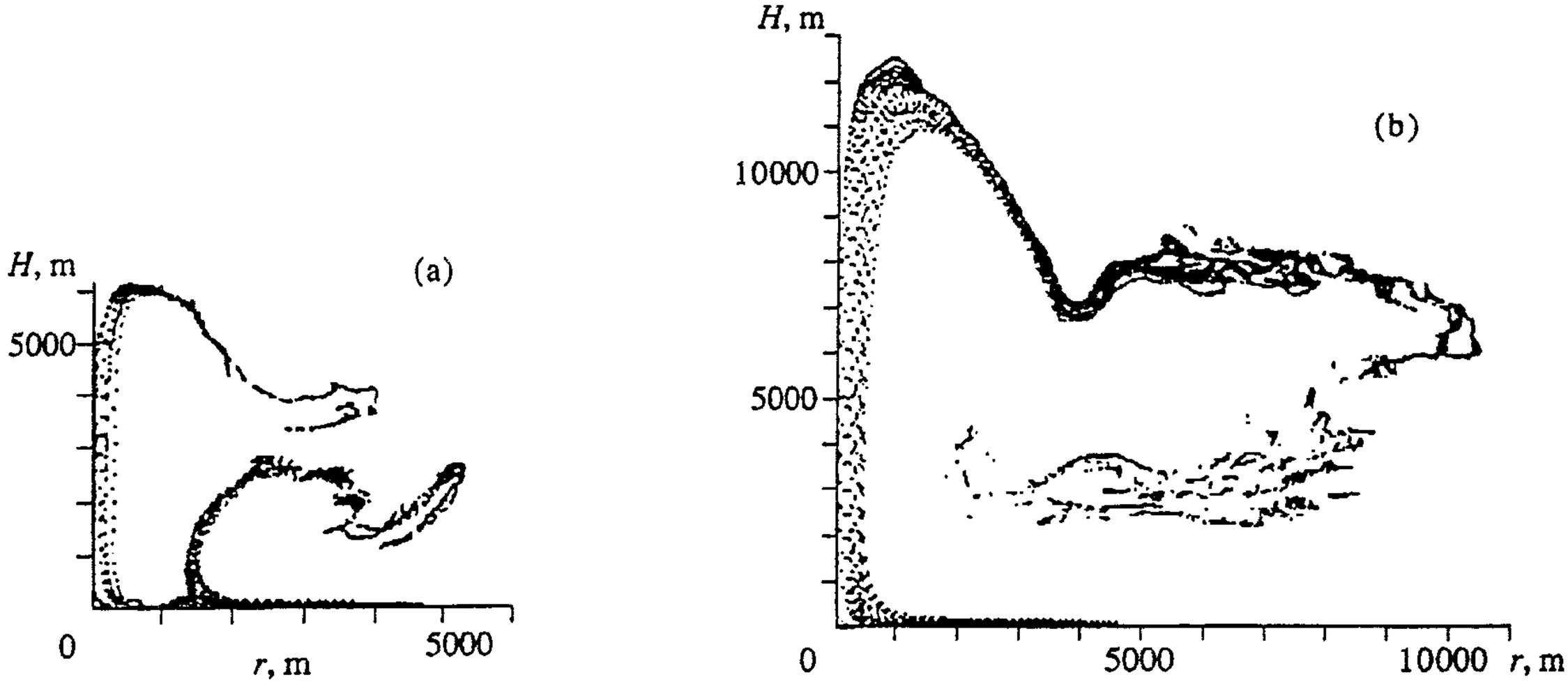

Fig. 1. Distribution of contaminant in the cloud, corresponding to the moments of time of: (a) 20 min, (b) 60 min. The fire center radius $R = 5$ km.

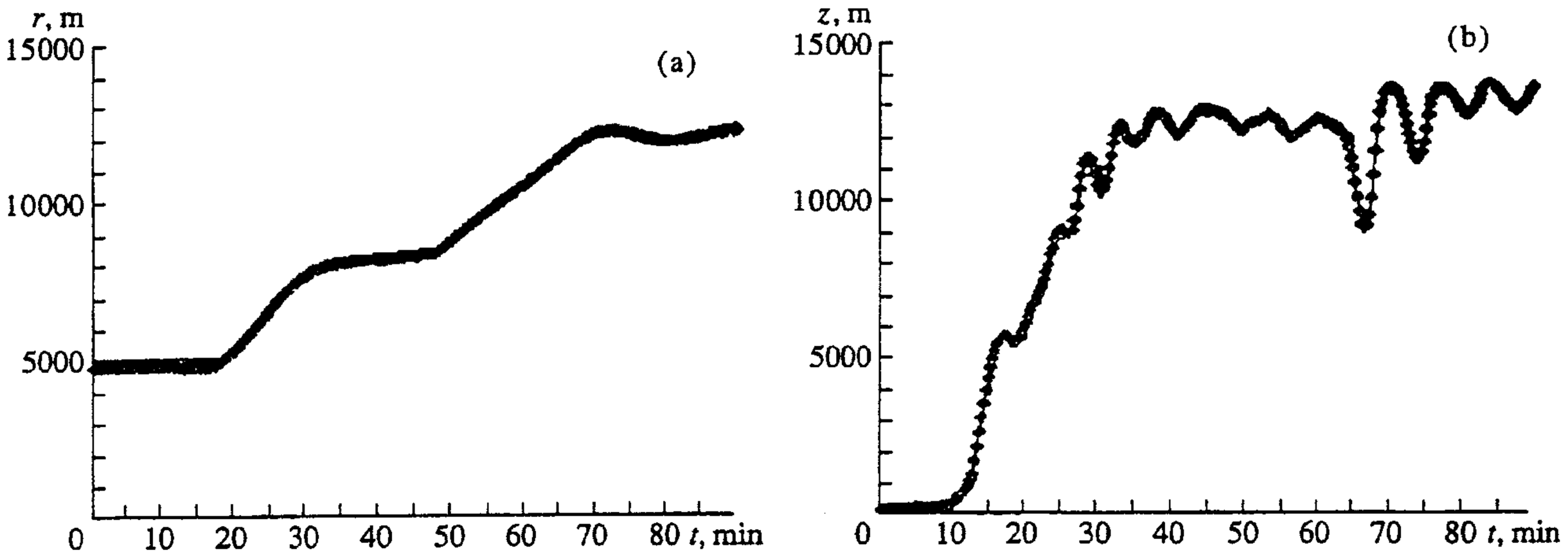

Fig. 2. The time dependence of (a) the maximum value of the cloud of contaminant and (b) the maximum altitude of rise of the contaminant. The fire center radius $R = 5$ km.

Note that the shift of the right-hand calculated boundary from the 30-km mark to 25 and 20 km did not cause a variation of the flow structure in the remaining region. This is indicative of the fact that the applied characteristic boundary conditions allow small disturbances to be released from the region without reflection from the boundary.

After the energy release source is cut off (60 min), the amplitude of oscillation of the top edge decreases significantly. As this takes place, the average altitude of the top edge corresponds to 14 km. The $r_{max}(t)$ and $z_{max}(t)$ relationships are shown in Fig. 4. While the altitude of the top edge barely increases with R, the radius of the cloud of the combustion products increases to approximately twice the radius of the fire center. The center radius $R = 11$ km corresponds to the maximum altitude of rise of the contaminant. After that, as R increases, the maximum altitude of the rise decreases. The shape of the contaminant cloud formed by the moments of 60 and 90 min is shown in Figs. 5a and 5b, respectively. As is seen from these drawings, in the case of $R = 11$ km at a later stage the contaminant propagates mainly at the altitude of 3 km. After the source is cut off, a noticeable sagging of the cloud is observed in the vicinity of the axis of symmetry, and this agrees with the experimental data of [10].

The dependence of z_{max} on q_f before $R = 11$ km is in good agreement with the well-known formula for a point source [14],

$$z_{max} = A q_f^{1/4}, \qquad (2)$$

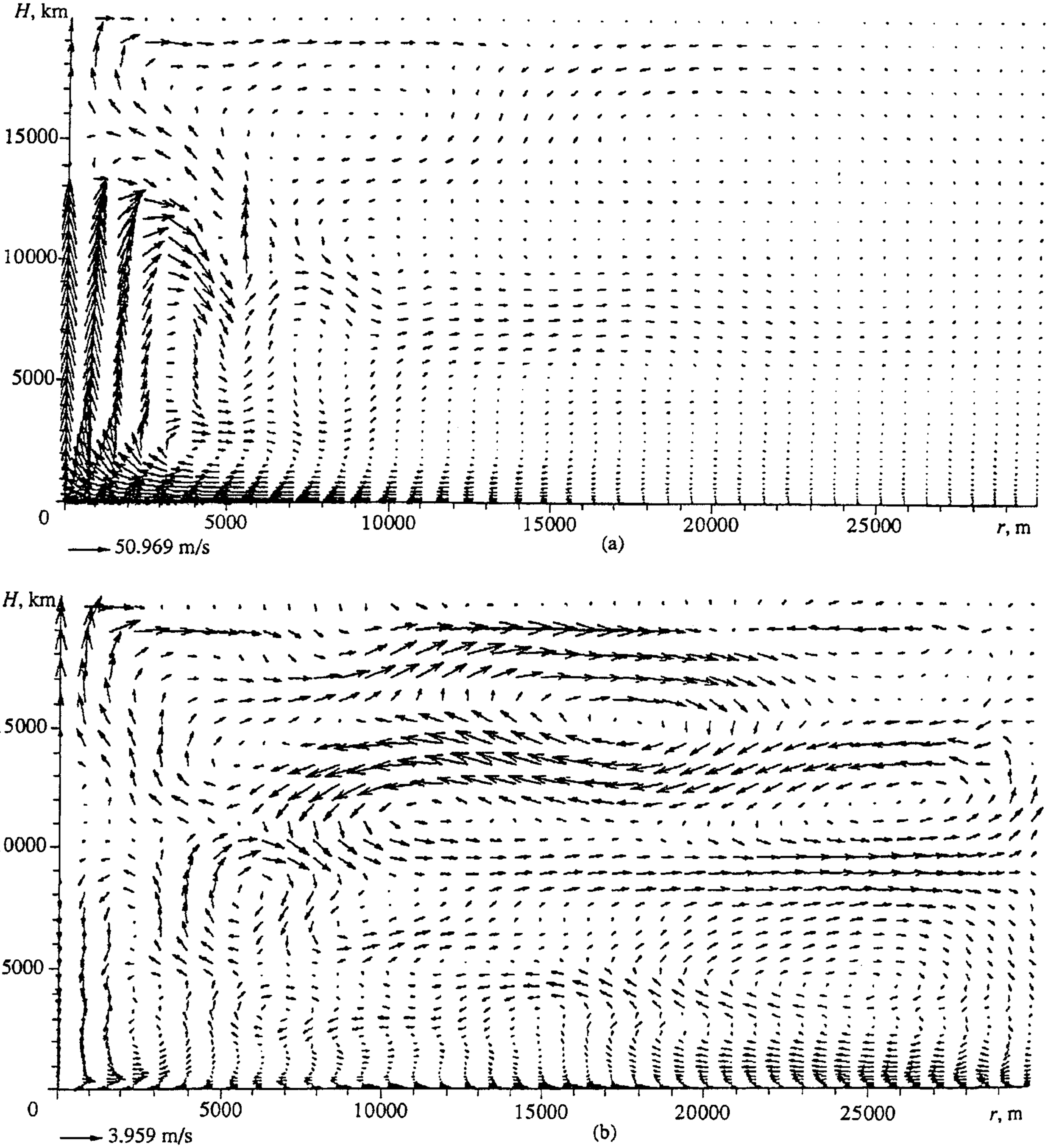

Fig. 3. The velocity field in the cloud of combustion products for the moments of time (a) 60 min, (b) 90 min. The fire center radius $R = 11$ km.

where z_{max} is measured in km and q_f in MW. According to the data of [15], $A = 0.255$ and according to the data of [16], $A = 0.31$. In [5], a conclusion is made that at $R = 5$ km, the value of $A = 0.255$ gives an estimation from below for the hovering height of the convective column, while $A = 0.31$ gives an estimation from above. The Table presents the values of z_{max} calculated by formula (2) and corresponding to the values of A equal to 0.255 and 0.31, as well as the values of z_{max} obtained in the form of the coordinate of the top edge of the cloud with due

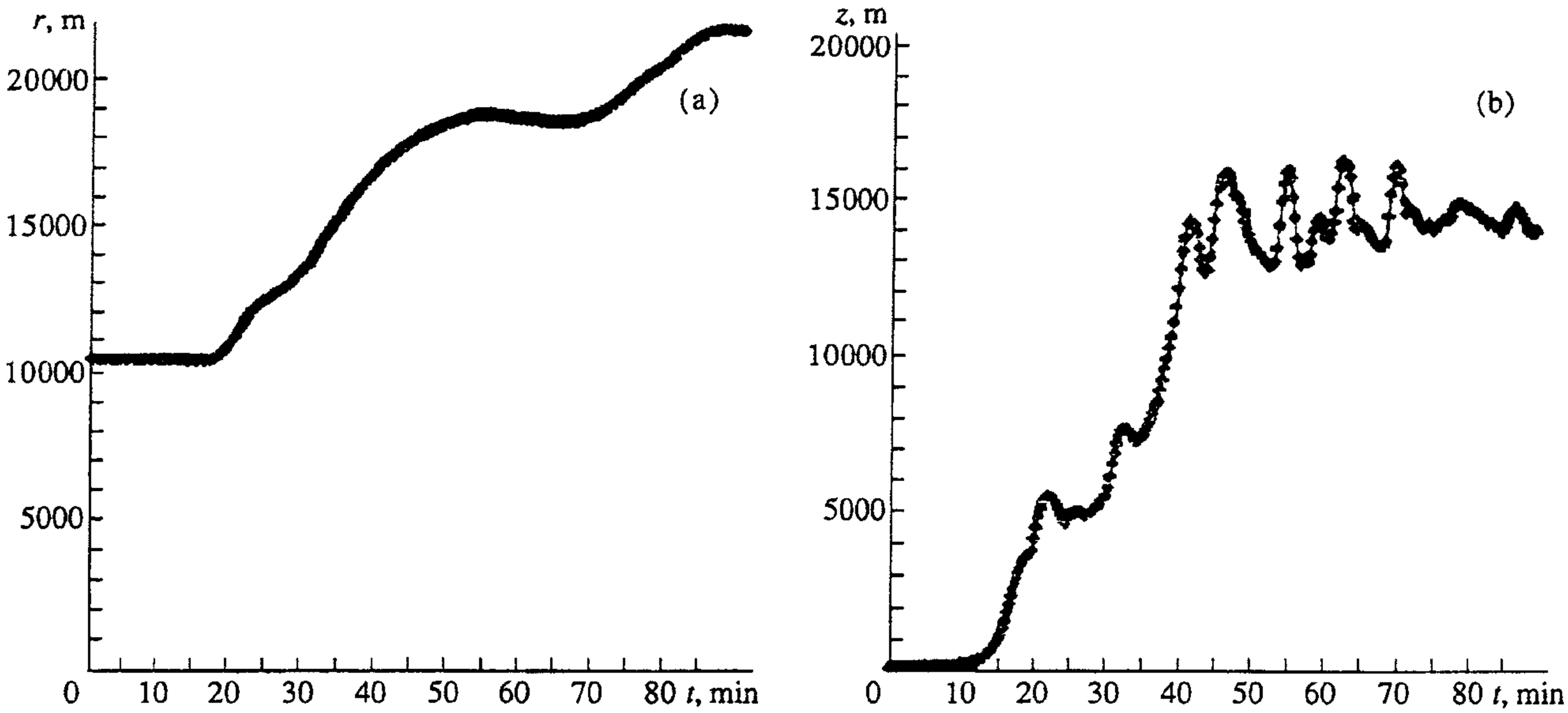

Fig. 4. The time dependence of (a) the maximum radius of the cloud of contaminant and (b) the maximum altitude of rise of the contaminant. The fire center radius $R = 11$ km.

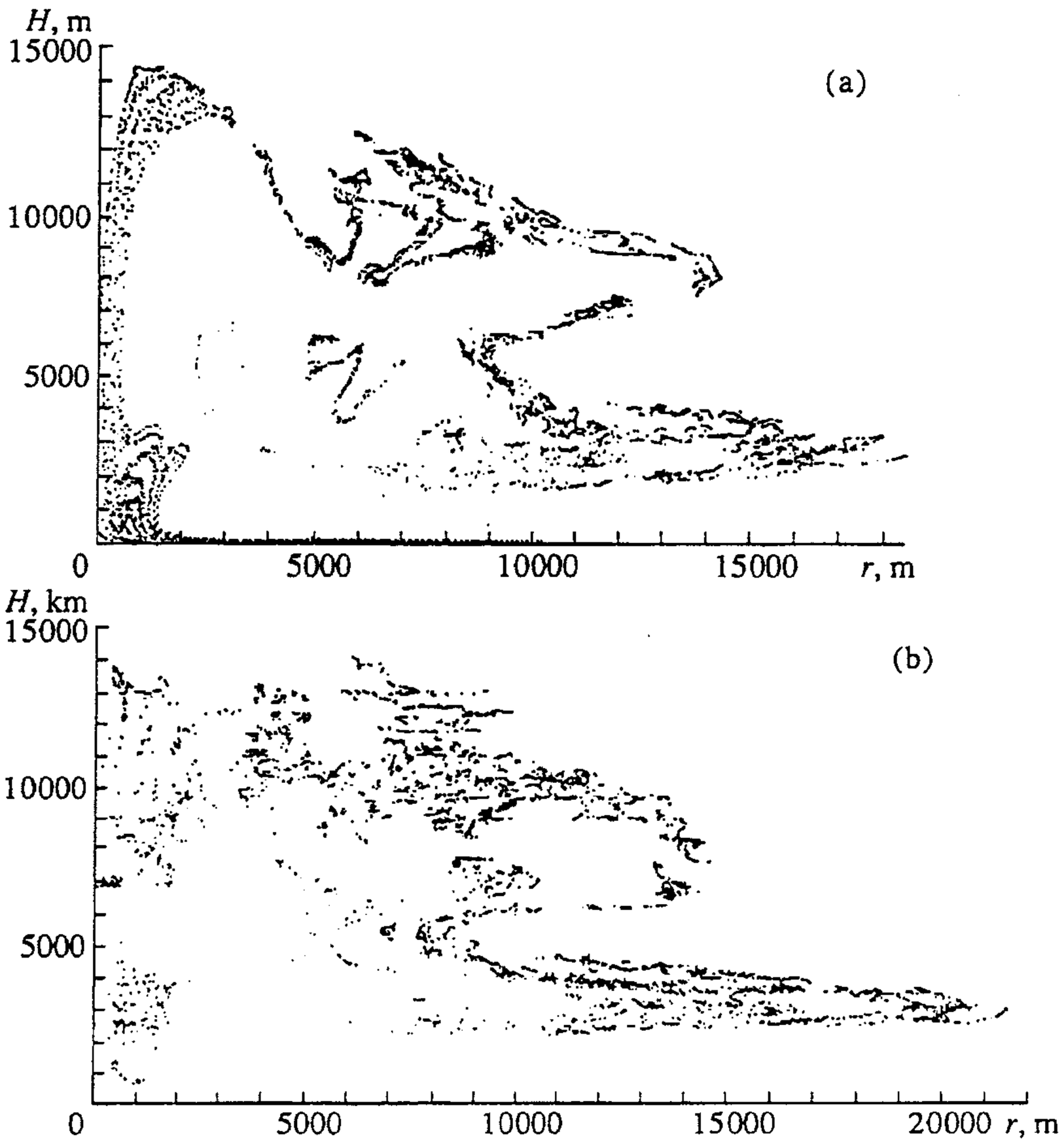

Fig. 5. Distribution of contaminant in the cloud corresponding to the moments of time: (a) 60 min, (b) 90 min. The fire center radius $R = 11$ km.

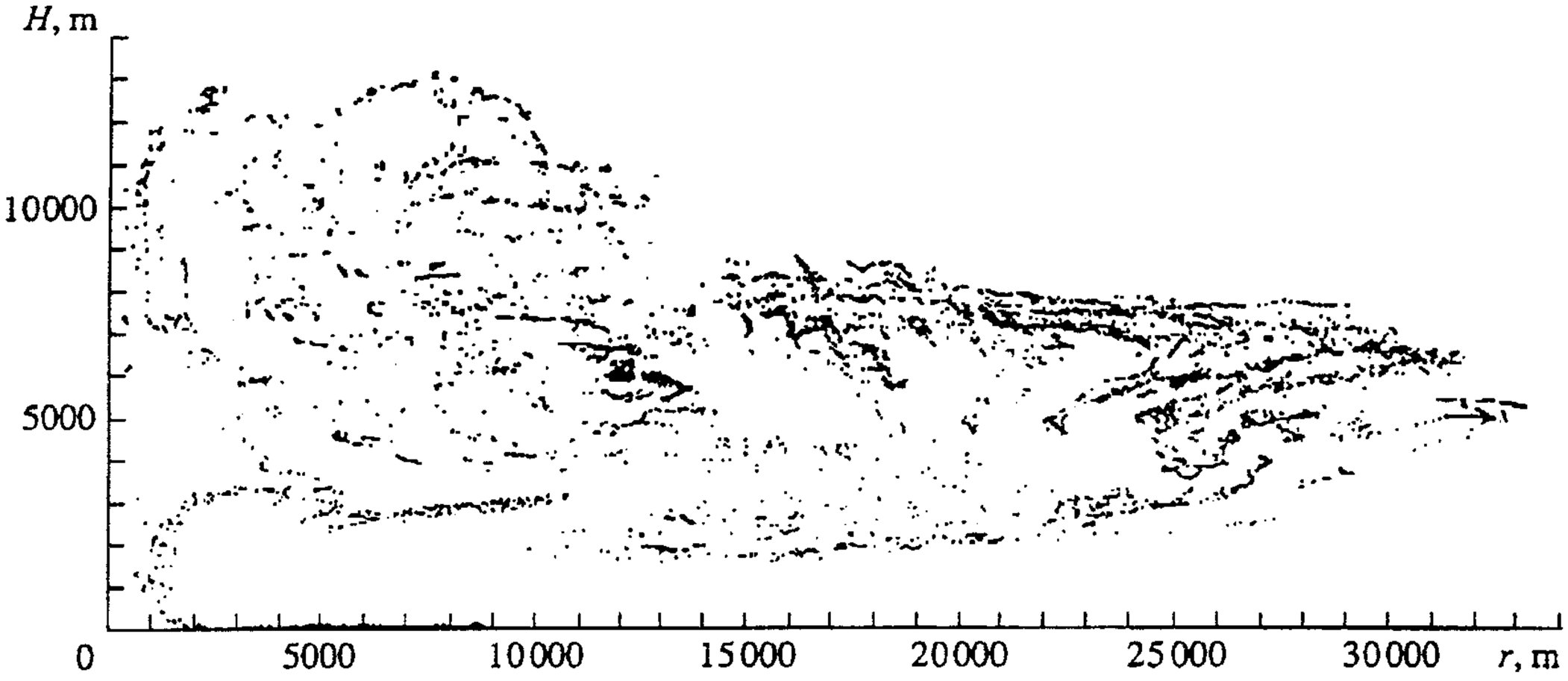

Fig. 6. Distribution of contaminant in the cloud at the moment of time of 80 min. The fire center radius $R = 22$ km.

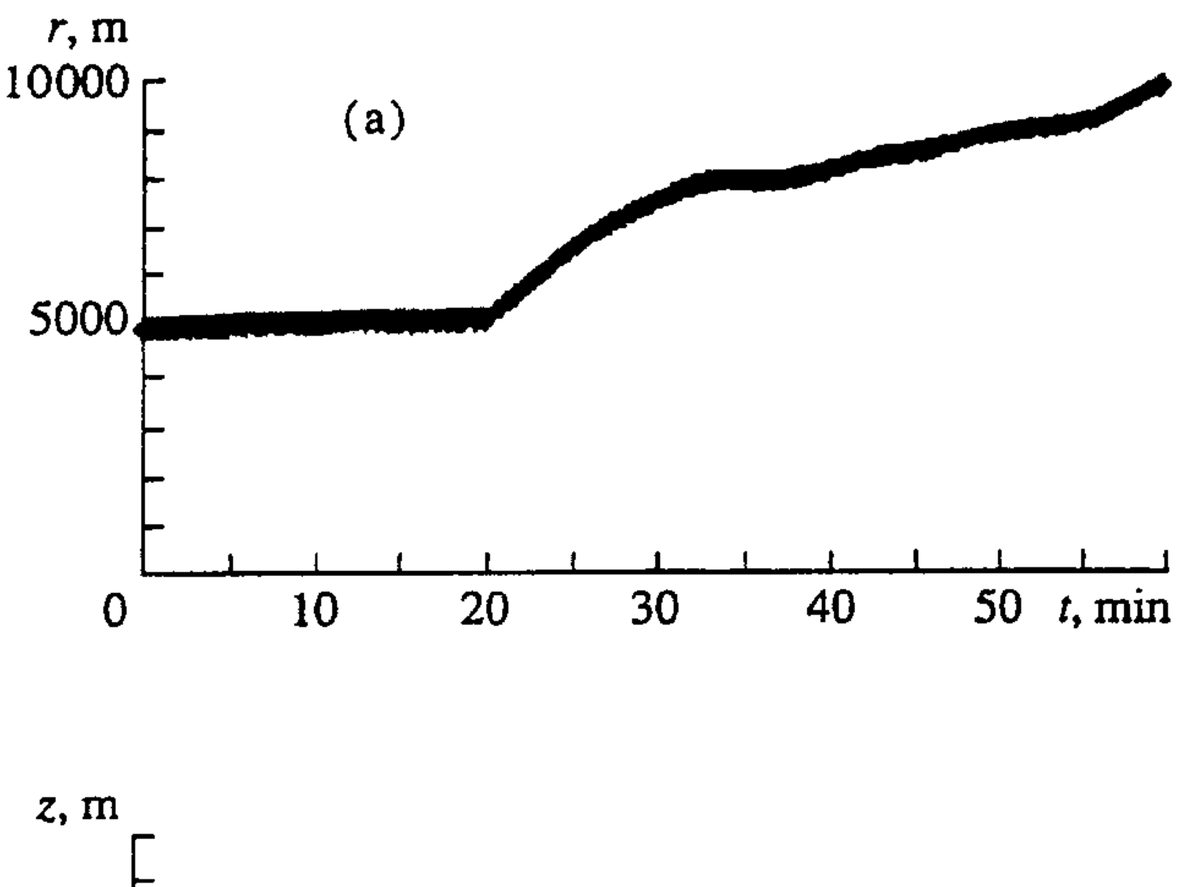

Fig. 7. The time dependence of (a) the maximum radius of the cloud of contaminant and (b) the maximum altitude of rise of the contaminant at constant values of the coefficient of turbulent viscosity and the Reynolds number $\mathrm{Re} = 5 \times 10^3$. The fire center radius $R = 5$ km.

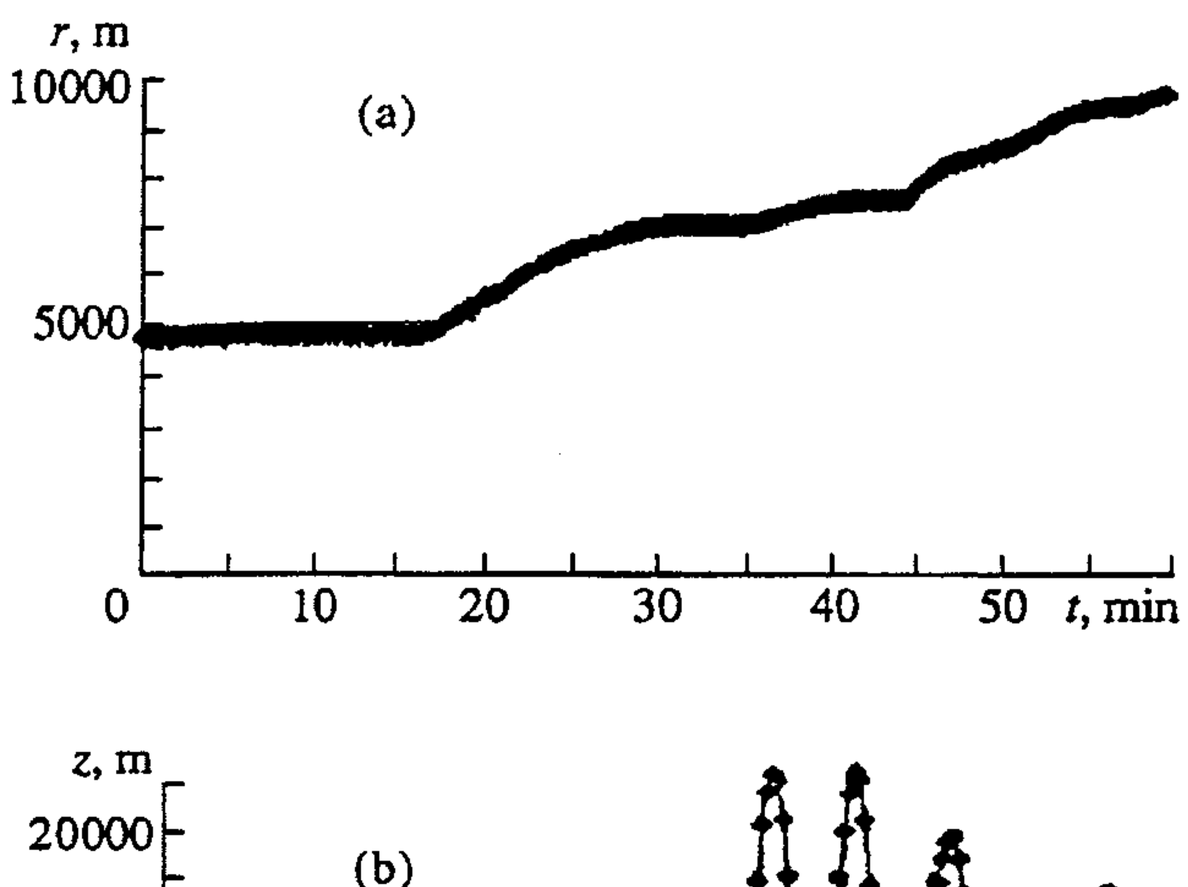

Fig. 8. Ditto. The Reynolds number $\mathrm{Re} = 10^4$. The fire center radius $R = 5$ km.

Table 1

R	$z_{max}(A = 0.255)$	$z_{max}(A = 0.31)$	$z_{max}^{(1)}$	$z_{max}^{(2)}$
5	11.3	13.4	11.3	13
8	14.4	17.5	11.9	15
11	16.8	20.5	12.9	16.2

regard for of its oscillation so that $z_{max}^{(1)} \le z_{max} \le z_{max}^{(2)}$.

It is clear from Table 1 that, while for $R = 5$ km formula (2) with the values of A equal to 0.255 and 0.31 indeed gives an accurate estimation from below and from above for the altitude of the top edge with due regard for its oscillation with time, for $R = 8$ km and $R = 11$ km this estimation does not hold. For the latter two values of R, the value of $A = 0.255$ is more appropriate, in which case formula (2) provides the estimation from above of the altitude of rise of the convective column.

Starting from $R = 11$ km, relation (2) corresponding to the point source is violated considerably. In the case of $R = 22$ km and $R = 33$ km, the maximum altitude of rise of the contaminant is equal to 16 and 15 km, respectively. After cutting off the energy release source, the altitude of rise of the convective column decreases by 3 km. The shape of the contaminant cloud for $R = 22$ km and $t = 80$ min is shown in Fig. 6.

Therefore, the maximum altitude of rise of the combustion products is 16 km with a variable fire area, and this has a significant effect on the amount of aerosol emitted into the atmosphere. The formation of a contaminant cloud at the tropopause altitude is attributed to the effect of dissipative processes linked with the flow turbulization. Figures 7 and 8 give the $z_{max}(t)$ relationships for the data corresponding to Figs. 1 - 3, but the coefficient of turbulent viscosity ν_t was set constant so that the Reynolds number Re assumed constant values of 5×10^3 and 10^4, respectively. It is evident that, in the case of a weak effect of the dissipative processes or their absence, the emission of contaminants into the atmosphere would occur even at $R = 5$ km.

ACKNOWLEDGMENTS

We are grateful to A.T. Onufriev for the formulation of the problem and useful discussion of the results obtained.

REFERENCES

1. Budyko, M.I., Golitsyn, G.S., and Izrael, Yu.A., *Global'nye Klimaticheskie Katastrofy* (Global Climatic Catastrophes), Moscow: Gidrometeoizdat, 1985.
2. Grishin, A.M., *Matematicheskoe Modelirovanie Lesnykh Pozharov i Novye Sposoby Bor'by s Nimi* (Mathematical Modeling of Forest Fires and New Methods of Fighting them), Novosibirsk: Nauka, 1992.
3. Kopylov, N.P., Ryzhov, A.M., and Khasanov, I.R., *Fiz. Goreniya Vzryva*, 1985, no. 5, p. 51.
4. Small, R.D. and Heires, K.E., *J. Appl. Meteorol.*, 1988, vol. 27, no. 5, p. 654.
5. Gostintsev, Yu.A., Kopylov, N.P., Ryzhov, A.M., and Khasanov, I.R., *Izv. Ross. Akad. Nauk, Mekh. Zhidk. Gaza*, 1990, no. 4, p. 47.
6. Gostintsev, Yu.A., Kopylov, N.P., Ryzhov, A.M., and Khasanov, I.R., *Fiz. Goreniya Vzryva*, 1991, no. 6, p. 10.
7. Gostintsev, Yu.A., Makhviladze, G.M., and Novozhilov, V.B., *Izv. Ross. Akad. Nauk, Mekh. Zhidk. Gaza*, 1992, no. 1, p. 17.
8. Tolstykh, A.I., *Kompaktnye Raznostnye Skhemy* (Compact Difference Schemas), Moscow: Nauka, 1990.
9. Muzafarov, I.F. and Utyuzhnikov, S.V., *Mat. Model.*, 1993, vol. 5, no. 3, p. 77.
10. Balabanov, V.A., Meshkov, M.A., Onufriev, A.T., Safarov, N.A., Safarov, R.A., and Skorovarov, V.E., in: *Tezisy Dokl. I Rossiiskaya Natsional'naya Konferentsiya* (Abstracts of Papers to the Ist Russian National Conference), 1994.
11. Penner, J.E., Haselman, L.C., and Edwards, L.L., *AIAA Publ.*, 1985, vol. 459, p. 1.
12. Muzafarov, I.F. and Utyuzhnikov, S.V., Application of Compact Difference Schemas to Solution of Quasi-Linear Complex Problem for Hyperbolic and Parabolic Systems of Equations, *Preprint of Moscow Physicotech. Inst.*, Moscow, 1994, no. 2.
13. Gossard, E. and Houk, T., *Volny v Atmosfere* (Waves in the Atmosphere), Moscow: Mir, 1978.
14. Morton, B.R., Taylor, G.T., and Turner, Y.S., *Proc. R. Soc. A*, 1956, vol. 234, no. 1196, p. 1.
15. Manins, P.C., *Atmos. Environ.*, 1985, vol. 19, no. 8, p. 1245.
16. Golitsyn, G.S., Gostintsev, Yu.A., and Solodovnik, A.F., *Prikl. Mat. Tekh. Fiz.*, 1989, no. 6, p. 61.